Int. J. Electrochem. Sci., 10 **(2015)** 2594 - 2601

International Journal of
ELECTROCHEMICAL
SCIENCE
www.electrochemsci.org

NiO Nanosheets with Large Specific Surface Area for Lithium-ion Batteries and Supercapacitors

Guoyong Huang[1], *Shengming Xu*[1,2,*], *Yongbin Cheng*[1,3], *Wenjing Zhang*[1], *Juan Li*[1], *Xiaohong Kang*[3,*]

[1]Institute of Nuclear and New Energy Technology, Tsinghua University, Beijing 100084, China
[2]Beijing Key Lab of Fine Ceramics, Tsinghua University, Beijing 100084, China
[3]School of Science, Beijing Jiaotong University, Beijing 100044, China
[*]E-mail: smxu@tsinghua.edu.cn; xhkang@bjtu.edu.cn

Received: 18 November 2014 / *Accepted:* 3 January 2015 / *Published:* 19 January 2015

In this study, irregular cubic phase NiO nanosheets (30.0-100.0 nm in width, 10.0-13.0 nm in thickness) with large specific surface area (120.5 m^2g^{-1}) have been synthesized for both Li-ion batteries and supercapacitors. The superior electrochemical performance including large reversible capacities, high specific capacitance and good cycle stability has been proved: the initial discharge capacity is 1827.7 $mAhg^{-1}$ and the reversible capacity is still about 560.0 $mAhg^{-1}$ after 50 cycles at 400 mAg^{-1}; the specific capacitance is as high as 1092.8 Fg^{-1} at 4 Ag^{-1} and the specific capacitance retention ratio is about 70.8% after 3000 cycles at 16 Ag^{-1}.

Keywords: NiO, Nanosheet, Lithium-ion battery, Supercapacitor, Energy storage and conversion

1. INTRODUCTION

NiO, one of important transition metal oxides, is widely used in many areas such as catalysis, gas sensors, magnetic and electrochemical materials [1-4]. Remarkably, due to the chemical and thermal stability, low cost and environmental friendliness, it has been popularly considered as a promising electrode in Li-ion batteries (LIBs) and supercapacitors (SCs) [5-8]. And the morphology, size and crystallinity of materials usually greatly influence the electronic properties. In order to find out special electrode materials with good performance, all kinds of NiO have been prepared and reported. For example, mesoporous NiO nanosheet networks (~ 5 μm in thickness) exhibits high first discharge capacity (~ 830 $mAhg^{-1}$ at 0.2 C) and excellent rate capability (~ 500 $mAhg^{-1}$ at 5 C) [9]; high-quality ultra-thin NiO nanosheets (< 2 nm in thickness) show a high reversible lithium storage capacity of 715 $mAhg^{-1}$ at 200 mAg^{-1} after 130 cycles [10]; the specific capacitances of loose-packed

NiO nano-flakes are 942 Fg^{-1}, 804 Fg^{-1}, 696 Fg^{-1} and 613 Fg^{-1} at 5 mA, 10 mA, 20 mA and 30 mA, respectively [11]; single-crystalline NiO nanosheet arrays exhibit a high specific capacitance (674 Fg^{-1} at 1 Ag^{-1}) and good cycling stability (93.5% capacitance retention after 5000 cycles) [12]. However, the reports about NiO powders used in both LIBs and SCs at the same time are very rare. Therefore, it is necessary to do research about the electrochemical performance of special morphological NiO powders in these two areas, and it is meaningful to do further research about NiO electrode with higher energy density, better cycling stability and enhanced rate capability. Herein, in this paper, through hydrothermal method followed by thermal treatment, irregular NiO nanosheets with large specific surface area have been synthesized by controlling the dosages of urea and triethanolamine for both LIBs and SCs, and the performance was evaluated by electrochemical measurements.

2. EXPERIMENTAL SECTION

Synthesis of Samples. $Ni(CH_3COO)_2•4H_2O$ (2.49 g), $CO(NH_2)_2$ (3.00 g) and triethanolamine (TEA) ($(HOCH_2CH_2)_3N$, 2.00 g) were dissolved in deionized water under vigorous stirring to obtain 100 ml transparent solution. It was then transferred into a Teflon-lined stainless steel autoclave (140 ml), and a thermal treatment was performed for the sealed autoclave in an electric oven at 160 °C for 10 h. After reaction, the green powders in the autoclave were collected and washed by deionized water and pure ethanol before being dried in a vacuum oven at 60 °C for 24 h. In order to get NiO, another thermal treatment was performed in air at 600 °C for 10 h with a heating ramp of 10 $°C·min^{-1}$. Then, the powders were collected again for further characterization.

Characterization of Samples. The crystal phase and morphology were characterized by X-ray powder diffraction (XRD) (Rigaku, D/Max-2000), scanning electron microscope (SEM) (JEOL, JSM 5500), transmission electron microscope (TEM) (JEOL, JSM 2011) and atomic force microscope (AFM) (Bruker, Dimension Icon). And the specific surface area was measured by the specific surface area and porosity analyzer (Micromeritics, Gemini VII 2390) through the nitrogen adsorption isotherm measurement data by Brunauer-Emmett-Teller (BET) method. One of working electrode was composed of NiO, acetylene black (ATB) and polytetrafluoroethylene (PTFE) with a weight ratio of NiO/ATB/PTFE = 7:2:1 (lithium metal as the reference electrode), and its capacity was measured in the range of 0.01-3.00 V (*vs*. Li^+/Li) at 25 °C by electrochemical test instrument (Land, CT2001A); the other one was composed of pure NiO powders with the electrolyte of KOH (1 $molL^{-1}$) aqueous solution in a three-electrode configuration (saturated Ag/AgCl as the reference electrode and Pt sheet as the counter electrode), and its specific capacitance was measured in the range of 0.01-0.40 V (*vs*. Ag/AgCl) at 25 °C by electrochemical workstation (CH Instruments, CHI 660E).

3. RESULTS AND DISCUSSION

The X-ray powder diffraction (XRD) patterns of samples are shown in Fig. 1. The diffraction peaks of precursor agree well with the standard pattern of cubic phase $Ni(HCO_3)_2$ (JCPDS no.15-

0782), while all of diffraction peaks of product are indexed as a cubic phase NiO with good crystallinity and purity (JCPDS no.71-1179). The specific surface area of NiO powders is about 120.5 m^2g^{-1} calculated based on the nitrogen adsorption isotherm measurement data by BET method (Fig. 2).

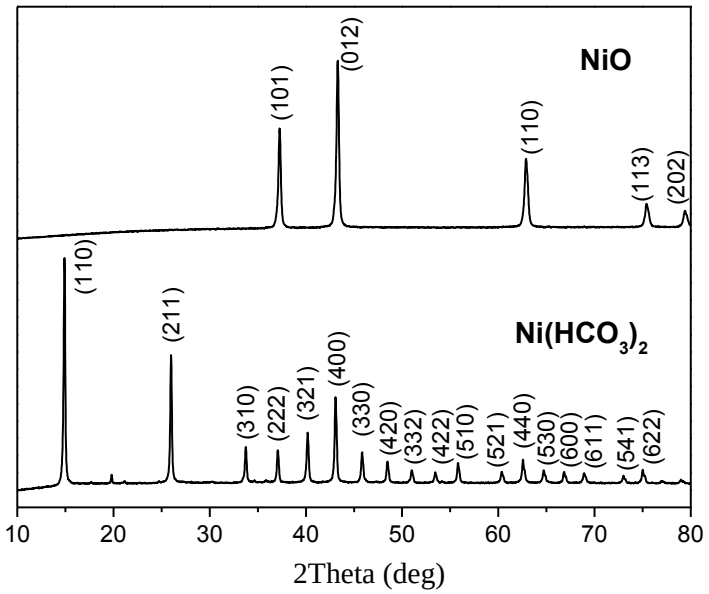

Figure 1. XRD patterns of precursor ($Ni(HCO_3)_2$) and product (NiO)

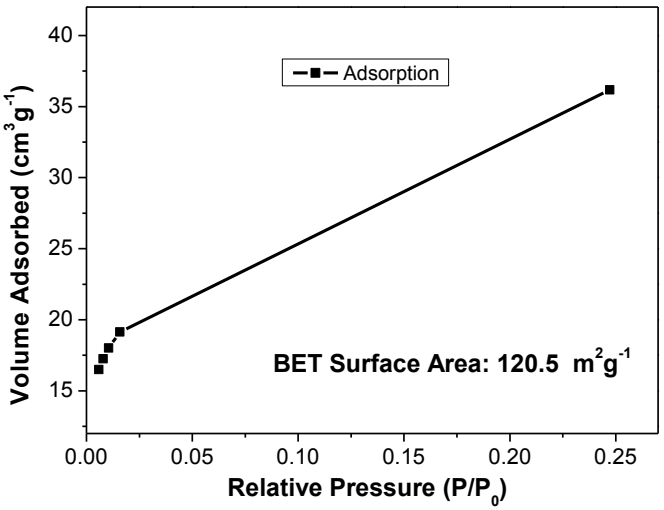

Figure 2. N_2 adsorption isotherm of NiO powders

Meanwhile, the scanning electron microscope (SEM), transmission electron microscope (TEM) and high-resolution transmission electron microscope (HRTEM) images are shown in Fig. 3. It indicates that the NiO powders are composed of many irregular monodispersed nanosheets (30.0-100.0 nm in width) by SEM images (Fig. 3a and Fig. 3b) and TEM image (Fig. 3c). In addition, the lattice fringes with lattice spacings of 0.21 nm and 0.24 nm match well with the (012) and (101) planes of cubic phase NiO shown by HRTEM images (Fig. 3d-3f). In a word, the NiO nanosheets maybe possess

the single-crystal structure. Through the atomic force microscopy (AFM) observation (Fig. 4), the thickness of NiO nanosheets is about 10.0-13.0 nm.

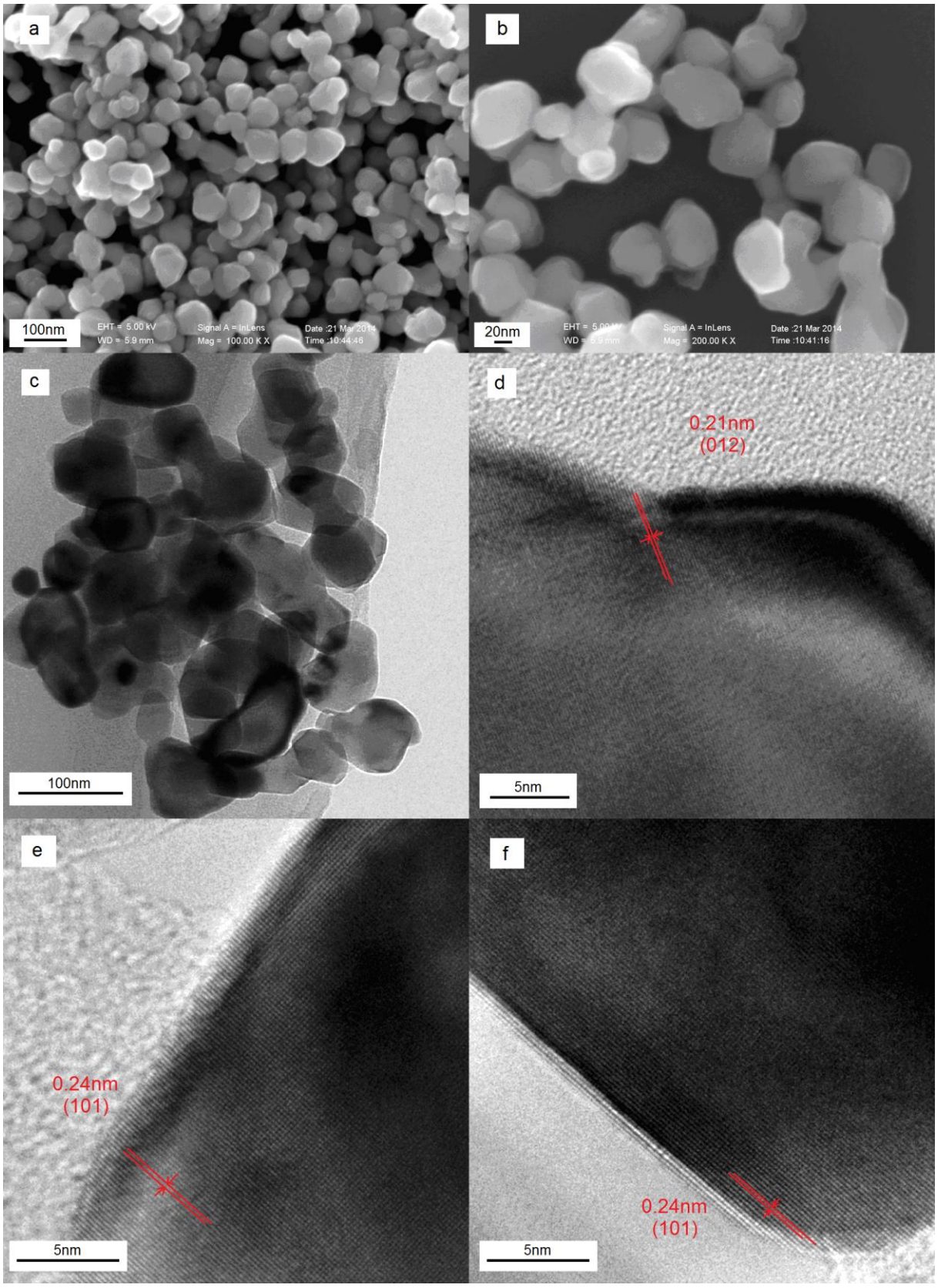

Figure 3. (a) and (b) SEM images, (c) TEM image and (d-f) HRTEM images of NiO powders

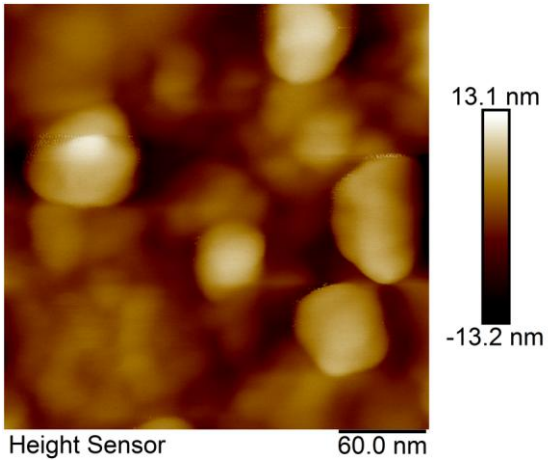

Figure 4. AFM image of NiO powders

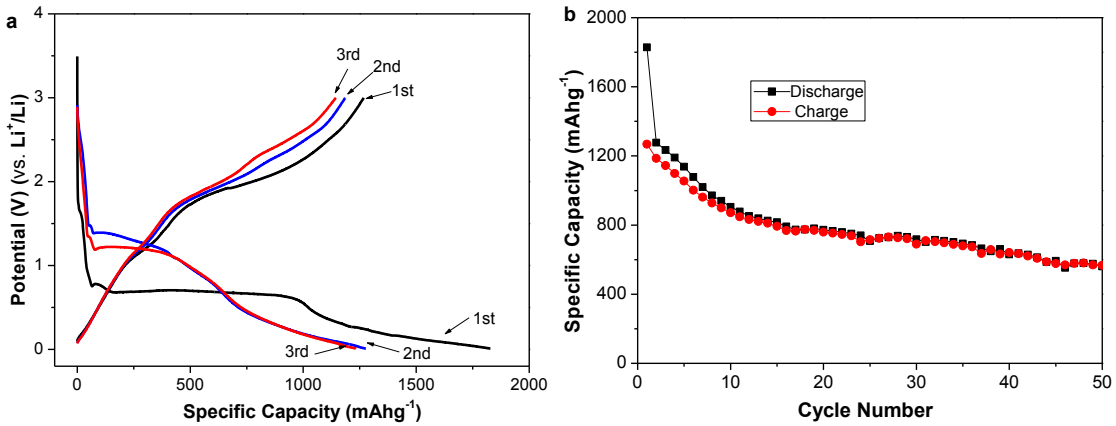

Figure 5. (a) Discharge and charge profiles of first three cycles and (b) Cycling performance of NiO electrode through coin cells in the range of 0.01-3.00 V (*vs.* Li^+/Li) at 400 mAg^{-1}

The electrochemical performance of NiO as an anode material of LIBs was evaluated through coin cell. The discharge and charge profiles of the first three cycles (lithium metal as the reference electrode) in the voltage range of 0.01-3.00 V (*vs.* Li^+/Li) at 400 mAg^{-1} are shown in Fig. 5a. In the initial discharge curve, the potential value quickly reduces to a plateau (~ 0.65 V), then gradually falls to the cut-off voltage (0.01 V), which may be caused by the conversion from NiO to Ni [Eq. (1)]; in the initial charge curve, the potential slowly increases to the peak voltage (3.00 V), corresponding to the reduction of NiO to Ni [Eq. (2)] [13, 14]. And the first discharge and charge capacities are as high as 1827.7 $mAhg^{-1}$ and 1267.5 $mAhg^{-1}$, respectively. It is a pity that the first irreversible capacity loss is about 30.7%, which may be ascribed to the formation of irreversible SEI film as previous reports [15, 16]. After the first cycle, the change trends of discharge/charge curves (the second and third cycles) are similar, indicating that the reduction/oxidation reactions become stable [17-19]. The cycling performance of the NiO nanosheets at 400 mAg^{-1} shown in Fig. 5b, the discharge capacity falls quickly from the top value to 816.5 $mAhg^{-1}$ at the first 15 cycles, and it slowly decreases to about 560.0 $mAhg^{-1}$ at the 50th cycle. But the Coulombic efficiency of every cycle (except the first one) is more than

92%. Therefore, the NiO nanosheets possess a large initial discharge/charge capacities and good cycle stability.

$$NiO + 2Li^+ + 2e^- \rightarrow Ni + Li_2O \quad (1)$$

$$Ni + Li_2O \rightarrow NiO + 2Li^+ + 2e^- \quad (2)$$

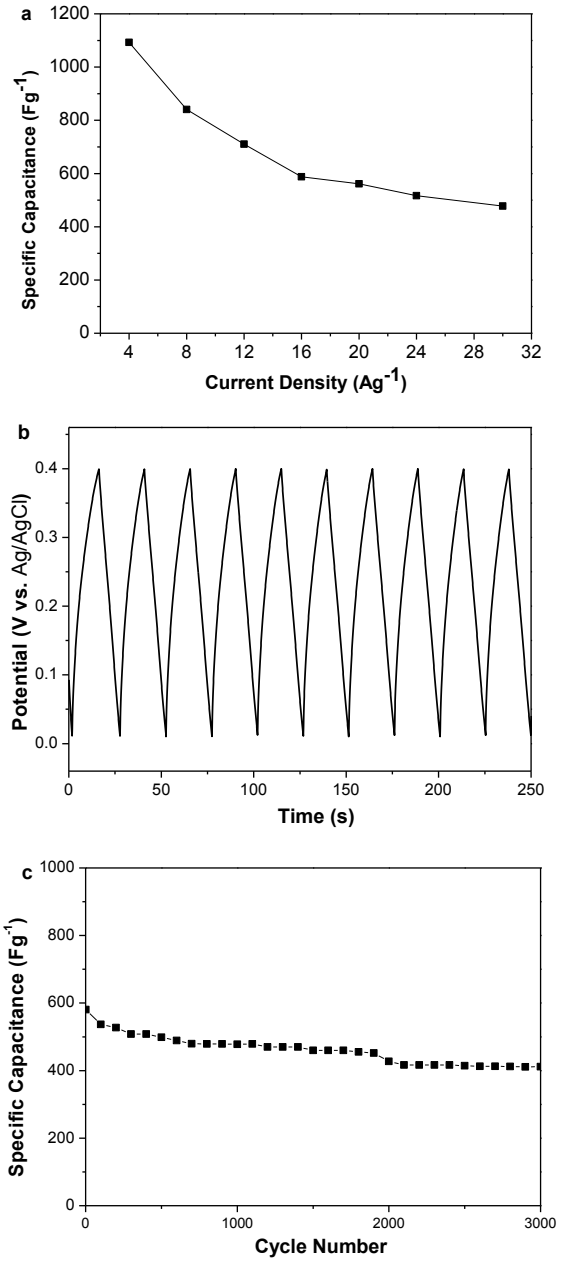

Figure 6. (a) Specific capacitances of NiO electrode with three-electrode configuration at different current densities, (b) Discharge and charge profiles of first 10 cycles in the range of 0.01-0.40 V (*vs*. Ag/AgCl) at 16 Ag^{-1} and (c) Cycle performance of NiO electrode with three-electrode configuration at 16 Ag^{-1}

On the other hand, the electrochemical performance of NiO for SCs was investigated through three-electrode configuration. It is shown that the relationship between the specific capacitance and the

current density in Fig. 6a. The specific capacitances of NiO nanosheets are 1092.8 Fg^{-1}, 804.8 Fg^{-1}, 710.7 Fg^{-1}, 587.6 Fg^{-1}, 561.5 Fg^{-1}, 516.6 Fg^{-1} and 477.8 Fg^{-1} at 4 Ag^{-1}, 8 Ag^{-1}, 12 Ag^{-1}, 16 Ag^{-1}, 20 Ag^{-1}, 24 Ag^{-1} and 30 Ag^{-1}, respectively. As the increase of the current density, the specific capacitance decreases quickly, especially at the high current density such as 24 Ag^{-1} and 30 Ag^{-1}, which may be ascribed to the increase of the internal diffusion resistance within the active material [12]. However, the initial specific capacitance retention ratio is about 65.0% from 4 Ag^{-1} to 16 Ag^{-1}, showing the good rate property of the NiO nanosheets. Fig. 6b shows the discharge and charge profiles of the representative first 10 cycles with three-electrode configuration in the voltage range of 0.01-0.40 V (*vs*. Ag/AgCl) at 16 Ag^{-1}. The shapes of the charge/discharge curves are almost unchanged during the whole process, suggesting that the NiO nanosheets are very suitable for supercapacitor applications [20, 21]. In addition, the cycle performance of pure NiO electrode at 16 Ag^{-1} with 3000 cycles is shown in Fig. 6c. At first, the specific capacitance of NiO nanosheets quickly falls to 508.4 Fg^{-1} after 400 cycles. Then, the specific capacitance keep a stable value between 500 Fg^{-1} and 450 Fg^{-1} till the 2000th cycle. At last, the specific capacitance retention ratio is still about 70.8% after 3000 cycles. It is proved again that the stable NiO nanosheets possess perfect electrochemical property.

There may be three advantages of this NiO material as follows: (1) its huge surface area increases the reaction interface between active materials and electrolyte [2, 14, 22]; (2) the nanoscale particles make diffusion length of lithium-ions to be shorter [10, 16, 23]; (3) the sheet structure can accommodate the volume expansion much better with lithium-ions inserting and extracting [2, 12, 21].

4. CONCLUSION

In summary, irregular cubic phase NiO nanosheets (30.0-100.0 nm in width, 10.0-13.0 nm in thickness) with big specific surface area (120.5 m^2g^{-1}) have been synthesized for both LIBs and SCs. The superior electrochemical performance including large reversible capacities, high specific capacitance and good cycle stability has been proved: the initial discharge and charge capacities are 1827.7 $mAhg^{-1}$ and 1267.5 $mAhg^{-1}$, and the reversible capacity is still about 560.0 $mAhg^{-1}$ after 50 cycles at 400 mAg^{-1}; the specific capacitances are as high as 1092.8 Fg^{-1} and 804.8 Fg^{-1} at 4 Ag^{-1} and 8 Ag^{-1}, and the specific capacitance retention ratio is about 70.8% after 3000 cycles at 16 Ag^{-1}.

ACKNOWLEDGEMENTS
This work was supported by the National Natural Science Foundation of China (Grant Nos. 51274130 and 51074096) and the program for Changjiang Scholars and Innovative Research Team in University (IRT13026).

References

1. L. Lin, T. Liu, B. Miao, W. Zeng, *Mater. Lett.*, 102-103 (2013) 43.
2. Q. Dong, S. Yin, C. Guo, X. Wu, N. Kumada, T. Takei, A. Miura, Y. Yonesaki, T. Sato, *Appl. Caral. B-Environ.*, 147 (2014) 741.

3. K.K. Purushothaman, I.M. Babu, B. Sethuraman, G. Muralidharan, *ACS Appl. Mater. Interfaces*, 5 (2013) 10767.
4. Q.X. Xia, K.S. Hui, K.N. Hui, D.H. Hwang, S.K. Lee, W. Zhou, Y.R. Cho, S.H. Kwon, Q.M. Wang, Y.G. Son, *Mater. Lett.*, 69 (2012) 69.
5. Y. Huang, X. Huang, J. Lian, D. Xu, L. Wang, X. Zhang, *J. Mater. Chem.*, 22 (2012) 2844.
6. G. Zhou, D. Wang, L. Yin, N. Li, F. Li, H. Cheng, *ACS Nano*, 4 (2012) 3214.
7. J.W. Lee, T. Ahn, J.H. Kim, J.M. Ko, J.D. Kim, *Electrochim. Acta*, 56 (2011) 4849.
8. J. Sun, W. Li, B. Zhang, G. Li, L. Jiang, Z. Chen, R. Zou, J. Hu, *Nano Energy*, 4 (2014) 56.
9. X. Wang, L. Qiao, X. Sun, X. Li, D. Hu, Q. Zhang, D. He, *J. Mater. Chem. A*, 1 (2013) 4173.
10. Y. Zhu, H. Guo, Y. Wu, C. Cao, S. Tao, Z. Wu, *J. Mater. Chem. A*, 2 (2014) 7904.
11. J.W. Lang, L.B. Kong, W.J. Wu, Y.C. Luo, L. Kang, *Chem. Commun.*, (2008) 4213.
12. M. Huang, F. Li, J.Y. Ji, Y.X. Zhang, X.L. Zhao, X. Gao, *CrystEngComm*, 16 (2014) 2878.
13. G.Y. Huang, S.M. Xu, Y. Yang, H.Y. Sun, Z.B. Li, Q. Chen, S.S. Lu, *Mater. Lett.*, 131 (2014) 236.
14. G.Y. Huang, S.M. Xu, S.S. Lu, L.Y. Li, H.Y. Sun, *ACS Appl. Mater. Interfaces*, 6 (2014) 7236.
15. G.Y. Huang, S.M. Xu, L.Y. Li, X.J. Wang, S.S. Lu, *Acta Phys.-Chim. Sin.*, 30 (2014) 1121.
16. G.Y. Huang, S.M. Xu, S.S. Lu, L.Y. Li, H.Y. Sun, *Electrochim. Acta*, 135 (2014) 420.
17. D. Xie, Q. Su, W. Yuan, Z. Dong, J. Zhang, G. Du, *J. Phys. Chem. C*, 117 (2013) 24121.
18. X. Liu, S.W. Or, C. Jin, Y. Lv, C. Feng, Y. Sun, *Carbon*, 60 (2013) 215.
19. R.A. Susantyoko, X. Wang, Q. Xiao, E. Fitzgerald, Q. Zhang, *Carbon*, 68 (2014) 619.
20. A.K. Mondal, D. Su, Y. Wang, S. Chen, G. Wang, *Chem. Asian J.*, 8 (2013) 2828.
21. W. Yu, X. Jiang, S. Ding, B.Q. Li, *J. Power. Sources*, 256 (2014) 440.
22. G.Y. Huang, S.M. Xu, J.L. Wang, L.Y. Li, X.J. Wang, *Acta Chim. Sinica*, 71 (2013) 1589.
23. H.Y. Sun, Y.G. Liu, Y.L. Yu, M. Ahmad, D. Nan, J. Zhu, *Electrochim. Acta*, 118 (2014) 1.